XVI International Conference on Computational Plasticity. Fundamentals and Applications
COMPLAS 2021
E. Oñate, D. Peric, M. Chiumenti and Eduardo de Souza Neto (Eds)

A MIXED FINITE ELEMENT FORMULATION FOR ELASTOPLASTICITY

M. NAGLER*, A. PECHSTEIN* AND A. HUMER*

* Institute of Technical Mechanics
Johannes Kepler University Linz
Altenberger Str. 69, 4040 Linz
e-mail: michaela.nagler@jku.at

Key words: mixed finite elements, elastoplasticity, variational principle

Abstract. The present paper provides a variational formulation for elastoplasticity as foundation of a novel mixed finite element formulation. The *tangential-displacement normal-normal-stress* (TDNNS) method, which is based on the Hellinger-Reissner type formulation, is extended from linear elasticity to plasticity. The second law of thermodynamics serves as basis for a thermodynamically consistent variational inequality. The notion of the dissipation inequality and a corresponding dissipation function are starting points rather than definitions of a yield function and a flow potential. Excellent performance and accuracy of the proposed method are demonstrated in several benchmark problems.

1 INTRODUCTION

Efficient simulation of thin-walled structures is already challenging in the range of elasticity but even more so in problems of elastoplasticity, as, e.g., the analysis of sheet metal forming processes. A discretization of thin-walled structures with standard finite element methods is adverse due to diverse locking phenomena such as shear locking or volume locking. In common finite element programs, reduced integration is used to circumvent these problems [1], which, however, might lead to *hourglass* instabilities. Alternatively, mixed finite element methods based on the Hellinger-Reissner or the Hu-Washizu principles [2, 3, 4] provide effective means to avoid locking phenomena. Mixed methods allow, in addition to the displacements, using stresses and/or strains as unknown fields. A mixed finite element method for nearly incompressible elasticity based on the theoretical framework of the Hellinger-Reissner principle is derived in [5]. Pechstein and Schöberl presented the *tangential-displacement normal-normal-stress* (TDNNS) method, which is based on the Hellinger-Reissner principle for elasticity, in [6]. It has been shown rigorously that TDNNS elements do not suffer from shear locking when modeling thin structures [7].

The aim of the present paper is to extend the TDNNS method to elastoplastic materials in small-strain regimes. The literature on elastoplasticity is huge; we refer to the monographs [8, 9, 10, 11, 12] for both theoretical and computational foundations. A common approach to solve elastoplastic problems is the application of the return-mapping algorithm, as suggested by [13, 14]. An elastic predictor gained from an elastic trial step is fol-

lowed by a plastic corrector. For a comprehensive exposition of return-mapping methods, we refer to Simo and Hughes [12]. In contrast to this intrinsically iterative approach, we aim at designing a thermodynamically consistent mixed variational formulation. Different formulations to describe elastoplastic material behavior in a thermodynamical framework are presented e.g. by Han and Reddy [9], Lubliner [8] or Srinivasa [15]. For the definition of a variational formulation the principle of maximum dissipation is of central importance in the field of plasticity. It states that among all possible processes the actual process is that which is most dissipative. Examples of using a mixed finite element formulation applied to elastoplasticity can be found in [16, 17].

In this work the TDNNS method is extended to plasticity based on a variational formulation for three-dimensional problems. The three independent degrees of freedom are the tangential component of the displacement, the normal component of the normal stress vector and the plastic strain. The present paper starts with the basic relations of the classical plasticity theory in Section 2. In Section 3 a thermodynamically consistent framework is introduced. The connection between the flow rule and the dissipation inequality is derived. Section 4 provides a brief overview of the variational formulation using the TDNNS method for elasticity with the extension to plasticity. Finally, Section 5 treats numerical investigations, which emphasize the performance of the TDNNS method.

2 Classical Plasticity Theory

In the following, we outline the basics of the classical rate-independent plasticity theory for small deformations following [12]. An additive decomposition of the total strain $\boldsymbol{\varepsilon}$ into an elastic part $\boldsymbol{\varepsilon}_e$ and a deviatoric plastic part $\boldsymbol{\varepsilon}_p$ is allowed for the assumption of small strains

$$\boldsymbol{\varepsilon} = \boldsymbol{\varepsilon}_e + \boldsymbol{\varepsilon}_p \qquad \text{with} \qquad \operatorname{tr} \boldsymbol{\varepsilon}_p = 0, \tag{1}$$

i.e., the volumetric part of plastic strains $\operatorname{tr} \boldsymbol{\varepsilon}_p$ is assumed to vanish. In classical plasticity theory, the following key elements are required:

- A scalar-valued *yield function* F defines the yield surface in stress space. The *yield condition* states that

$$F(\boldsymbol{\sigma}, \boldsymbol{\alpha}) \leq 0 \tag{2}$$

  where $\boldsymbol{\sigma}$ denotes the stress tensor and $\boldsymbol{\alpha}$ comprises *internal* variables such as the plastic strain $\boldsymbol{\varepsilon}_p$ and the accumulated plastic strain γ. The yield surface and yield function are usually assumed convex.

- A *flow potential* G relates the actual stress state $\boldsymbol{\sigma}$ and the direction of plastic flow

$$\dot{\boldsymbol{\varepsilon}}_p = \lambda \, \frac{\partial G}{\partial \boldsymbol{\sigma}}, \tag{3}$$

  where λ is usually referred to as consistency or Kuhn-Tucker parameter and $\dot{\boldsymbol{\varepsilon}}_p$ specifies the plastic strain rate. The consistency parameter λ cannot be negative due to the irreversible character of the plastic deformation. If the flow potential G and the yield function F coincide, the flow rule is called *associated*.

- A *consistency condition* for the yield condition (2) and the Kuhn-Tucker parameter (3), i.e.,
$$\lambda \geq 0, \quad F(\boldsymbol{\sigma}, \boldsymbol{\alpha}) \leq 0, \quad \lambda F(\boldsymbol{\sigma}, \boldsymbol{\alpha}) = 0, \tag{4}$$
ensures that the stress state remains on the yield surface during plastic loading.

In the case of perfect plasticity, the yield surface is independent of the state of plastic deformation. Two standard models, and a combination of both, are typically used for the modeling of a hardening response, i.e., an evolution of the yield surface based on plastic strains and their temporal evolution:

- *Isotropic hardening:* The yield surface keeps its shape but expands with increasing stress. The *von Mises* yield criterion can be expressed via
$$F^{iso} = \| \operatorname{dev} \boldsymbol{\sigma} \| - \frac{2}{3} H_0 \, \gamma - \sqrt{\frac{2}{3}} \, Y \leq 0, \tag{5}$$
where $\operatorname{dev} \boldsymbol{\sigma} := \boldsymbol{\sigma} - (\operatorname{tr} \boldsymbol{\sigma}) \mathbf{I}/3$ denotes the deviatoric part of the stress tensor with the second-order identity tensor $\mathbf{I}$; H_0 is the modulus of isotropic hardening, Y defines the yield stress and γ denotes the accumulated plastic strain rate
$$\gamma = \int_0^t \| \dot{\boldsymbol{\varepsilon}}_p(s) \| \, \mathrm{d}s. \tag{6}$$
The accumulated plastic strain is non-negative and monotonically increasing.

- *Kinematic hardening:* As opposed to isotropic hardening, size and shape of the yield surface remain fixed, but its origin may translate
$$F^{kin} = \left\| (\operatorname{dev} \boldsymbol{\sigma}) - \frac{2}{3} H_0 \, \boldsymbol{\varepsilon}_p \right\| - \sqrt{\frac{2}{3}} \, Y \leq 0. \tag{7}$$

- *Combined kinematic and isotropic hardening:* The extension to a combined isotropic/ kinematic hardening model is defined for $\theta \in [0, 1]$
$$F = \left\| (\operatorname{dev} \boldsymbol{\sigma}) - (1 - \theta) \frac{2}{3} H_0 \, \boldsymbol{\varepsilon}_p \right\| - \theta \frac{2}{3} H_0 \, \gamma - \sqrt{\frac{2}{3}} \, Y \leq 0. \tag{8}$$
The extremal values of θ correspond to the two special cases of hardening cited above, i.e., $\theta = 1$ for isotropic hardening $\theta = 0$ and for kinematic hardening.

3 Maximum Plastic Dissipation

The principle of maximum plastic dissipation plays a pivotal role within our considerations. Together with the second law of thermodynamics, it forms the foundation for the derivation of consistent constitutive equations that govern the stress response and the evolution of internal variables. Assuming isothermal conditions, the second law of

thermodynamics is formulated in terms of the Clausius-Duhem inequality, which requires the dissipation ξ, i.e., the rate of dissipated energy, to be positive:

$$\xi = \boldsymbol{\sigma} \cdot \dot{\boldsymbol{\varepsilon}} - \dot{\psi} \geq 0. \tag{9}$$

In the above relation, ψ denotes the stored energy density, which is also referred to as Helmholtz free energy. The Helmholtz free energy ψ is additively decomposed into reversible (elastic) and irreversible (plastic or hardening) contributions,

$$\psi = \psi_e(\boldsymbol{\varepsilon}_e) + \psi_p(\boldsymbol{\varepsilon}_p, \gamma), \tag{10}$$

where the plastic part ψ_p depends only on the internal variables. Substituting its rate, the (reduced) dissipation inequality (9) is recast into

$$\begin{aligned} \xi &= \left(\boldsymbol{\sigma} - \frac{\partial \psi_e}{\partial \boldsymbol{\varepsilon}_e}\right) : \dot{\boldsymbol{\varepsilon}}_e + \left(\boldsymbol{\sigma} - \frac{\partial \psi_p}{\partial \boldsymbol{\varepsilon}_p}\right) : \dot{\boldsymbol{\varepsilon}}_p - \frac{\partial \psi_p}{\partial \gamma}\, \dot{\gamma} \\ &= \left(\boldsymbol{\sigma} - \frac{\partial \psi_e}{\partial \boldsymbol{\varepsilon}_e}\right) : \dot{\boldsymbol{\varepsilon}} + \frac{\partial \psi_e}{\partial \boldsymbol{\varepsilon}_e} : \dot{\boldsymbol{\varepsilon}}_p - \frac{\partial \psi_p}{\partial \boldsymbol{\varepsilon}_p} : \dot{\boldsymbol{\varepsilon}}_p - \frac{\partial \psi_p}{\partial \gamma}\, \dot{\gamma} \geq 0. \end{aligned} \tag{11}$$

From the above relation, we identify stresses and dissipative driving forces dual to the harding variables as

$$\boldsymbol{\sigma} = \frac{\partial \psi_e}{\partial \boldsymbol{\varepsilon}_e}, \qquad \boldsymbol{q}_1 = -\frac{\partial \psi_p}{\partial \boldsymbol{\varepsilon}_p}, \qquad q_2 = -\frac{\partial \psi_p}{\partial \gamma}. \tag{12}$$

For a linear elastic material, the strain energy is assumed quadratic in the elastic strains $\boldsymbol{\varepsilon}_e = \boldsymbol{\varepsilon} - \boldsymbol{\varepsilon}_p$:

$$\psi_e = \frac{1}{2}(\boldsymbol{\varepsilon} - \boldsymbol{\varepsilon}_p) : \mathbb{C} : (\boldsymbol{\varepsilon} - \boldsymbol{\varepsilon}_p). \tag{13}$$

In the above relation, $\mathbb{C}$ denotes the fourth-order elasticity tensor, which, in the case of isotropy, can be expressed as

$$\mathbb{C} = \lambda\, \mathbf{I} \otimes \mathbf{I} + 2\mu\, \mathbf{1}, \tag{14}$$

where $\mathbf{1}$ the fourth-order symmetric identity tensor and λ, μ are the Lamè constants. The stress response follows from the general constitutive equation (12) as the derivate with respect to the elastic strains, i.e.,

$$\boldsymbol{\sigma} = \frac{\partial \psi_e}{\partial \boldsymbol{\varepsilon}_e} = \mathbb{C} : \boldsymbol{\varepsilon}_e. \tag{15}$$

The dissipation therefore follows as

$$\xi = -\frac{\partial \psi_p}{\partial \boldsymbol{\varepsilon}_p} : \dot{\boldsymbol{\varepsilon}}_p - \frac{\partial \psi_p}{\partial \gamma}\, \dot{\gamma} + \boldsymbol{\sigma} : \dot{\boldsymbol{\varepsilon}}_p \geq 0. \tag{16}$$

Hardening is characterized by including internal variables in the description of the yield surface. For linear kinematic hardening, the internal variable is equal to the plastic strain

tensor $\boldsymbol{\varepsilon}_p$; for isotropic hardening, the accumulated plastic strain γ serves as internal variable. Consequently, the (combined) free energy takes the following form

$$\psi_p(\boldsymbol{\varepsilon}_p, \gamma) = (1-\theta)\,\frac{1}{3}\,H_0\,\boldsymbol{\varepsilon}_p : \boldsymbol{\varepsilon}_p + \theta\,\frac{1}{3}\,H_0\,\gamma^2. \tag{17}$$

Within our thermodynamical approach, the yield function F is defined implicitly by the explicit choice of a dissipation function ξ. For the sake of brevity, we only consider kinematic hardening (i.e., $\theta = 0$) in the subsequent derivations. To realize the *von Mises* yield criterion in Eq. (7), a dissipation function is chosen as a positively homogeneous function of degree 1:

$$\xi = \sqrt{\frac{2}{3}}\,Y\,\|\dot{\boldsymbol{\varepsilon}}_p\|. \tag{18}$$

To reveal the connection of the dissipation function (18) and the yield criterion (7), we consider the reduced form of the dissipation inequality, Eq. (16), which is rewritten as

$$-\frac{\partial \psi_p}{\partial \boldsymbol{\varepsilon}_p} : \dot{\boldsymbol{\varepsilon}}_p + \boldsymbol{\sigma} : \dot{\boldsymbol{\varepsilon}}_p - \xi(\dot{\boldsymbol{\varepsilon}}_p) = 0. \tag{19}$$

Inserting the definition of the plastic part of the free energy for kinematic hardening, Eq. (17) and the dissipation function (18), the following form can be obtained

$$-\frac{2}{3}\,H_0\,\boldsymbol{\varepsilon}_p : \dot{\boldsymbol{\varepsilon}}_p + \boldsymbol{\sigma} : \dot{\boldsymbol{\varepsilon}}_p - \sqrt{\frac{2}{3}}\,Y\,\|\dot{\boldsymbol{\varepsilon}}_p\| = 0. \tag{20}$$

Assuming $\|\dot{\boldsymbol{\varepsilon}}_p\| \neq 0$, i.e., plastic loading occurs, we divide the above relation by $\|\dot{\boldsymbol{\varepsilon}}_p\|$,

$$-\frac{2}{3}\,H_0\,\boldsymbol{\varepsilon}_p : \frac{\dot{\boldsymbol{\varepsilon}}_p}{\|\dot{\boldsymbol{\varepsilon}}_p\|} + (\boldsymbol{\varepsilon} - \boldsymbol{\varepsilon}_p) : \mathbb{C} : \frac{\dot{\boldsymbol{\varepsilon}}_p}{\|\dot{\boldsymbol{\varepsilon}}_p\|} - \sqrt{\frac{2}{3}}\,Y = 0, \tag{21}$$

and rearrange it as

$$\frac{\dot{\boldsymbol{\varepsilon}}_p}{\|\dot{\boldsymbol{\varepsilon}}_p\|} : \left(\boldsymbol{\sigma} - \frac{2}{3}\,H_0\,\boldsymbol{\varepsilon}_p\right) = \sqrt{\frac{2}{3}}\,Y. \tag{22}$$

As the plastic strains are deviatoric, only the deviatoric part of the stresses contributes to the dissipation, i.e.,

$$\frac{\dot{\boldsymbol{\varepsilon}}_p}{\|\dot{\boldsymbol{\varepsilon}}_p\|} : \left(\operatorname{dev}(\boldsymbol{\sigma}) - \frac{2}{3}\,H_0\,\boldsymbol{\varepsilon}_p\right) = \sqrt{\frac{2}{3}}\,Y. \tag{23}$$

The norm of the above relation results in the well-known *von Mises* yield function for kinematic hardening:

$$\left\|(\operatorname{dev}\boldsymbol{\sigma}) - \frac{2}{3}\,H_0\,\boldsymbol{\varepsilon}_p\right\| = \sqrt{\frac{2}{3}}\,Y. \tag{24}$$

4 Finite element formulation

The TDNNS method was developed for linear elasticity in [6]. The method uses mixed finite elements which are based on the Hellinger-Reissner principle. In the Hellinger-Reissner formulation, the displacement vector together with the stress tensor are used as separate unknowns. The variational formulation is defined as follows

$$-\int_\Omega (\mathbb{S} : \boldsymbol{\sigma}) : \delta\boldsymbol{\sigma} \,\mathrm{d}\Omega + \int_\Omega \boldsymbol{\varepsilon} : \delta\boldsymbol{\sigma} \,\mathrm{d}\Omega + \int_\Omega \boldsymbol{\sigma} : \delta\boldsymbol{\varepsilon} \,\mathrm{d}\Omega = \int_\Omega \boldsymbol{f} \cdot \delta\boldsymbol{u} \,\mathrm{d}\Omega, \tag{25}$$

where $\boldsymbol{u}$ denotes the displacement field, $\boldsymbol{f}$ are body forces and $\mathbb{S} = \mathbb{C}^{-1}$ is the fourth-order compliance tensor.

In the TDNNS formulation, the tangential component of the displacement $\boldsymbol{u}_t$ and the normal component of the normal stress vector σ_{nn} serve as degrees of freedom. For the displacement, tangential-continuous elements proposed by Nedelec [18] are utilized. Elements for which the normal component of the normal stress vector is continuous were introduced by Pechstein and Schöberl [6]. Note that, for this choice, inter-element gaps in normal direction may arise, which must be treated correctly. To this end, the following variational formulation based on Eq. (25) is used

$$-\int_\Omega \boldsymbol{\sigma} : \mathbb{S} : \delta\boldsymbol{\sigma} \,\mathrm{d}\Omega + \langle \boldsymbol{\varepsilon}(\boldsymbol{u}), \delta\boldsymbol{\sigma}\rangle + \langle \boldsymbol{\varepsilon}(\delta\boldsymbol{u}), \boldsymbol{\sigma}\rangle = \int_\Omega \boldsymbol{f} \cdot \delta\boldsymbol{u} \,\mathrm{d}\Omega. \tag{26}$$

In Eq. (26), the integral is replaced by a duality product to account for the discontinuous displacement field

$$\begin{aligned} \langle \boldsymbol{\varepsilon}(\boldsymbol{u}), \boldsymbol{\sigma}\rangle &= \sum_T \left(\int_T \boldsymbol{\varepsilon}(\boldsymbol{u}) : \boldsymbol{\sigma} - \int_{\partial T} u_n \, \sigma_{nn} \right) \\ &= -\sum_T \left(\int_T \operatorname{div} \boldsymbol{\sigma} \cdot \boldsymbol{u} - \int_{\partial T} \boldsymbol{\sigma}_{nt} \cdot \boldsymbol{u}_t \right) = -\langle \operatorname{div} \boldsymbol{\sigma}, \boldsymbol{u}\rangle. \end{aligned} \tag{27}$$

In what follows, we present an extension of the TDNNS method to plasticity. To include $\boldsymbol{\sigma}$ and $\boldsymbol{\varepsilon}_p$ as variables, we introduce the enthalpy density h by a Legendre transformation of the Helmholtz free energy:

$$h(\boldsymbol{\sigma}, \boldsymbol{\varepsilon}_p) = \min_{\boldsymbol{\varepsilon}} (\psi(\boldsymbol{\varepsilon}, \boldsymbol{\varepsilon}_p) - \boldsymbol{\sigma} : \boldsymbol{\varepsilon}). \tag{28}$$

Considering the additive decomposition of the free Helmholtz energy in Eq. (10) and inserting Eqs. (13) and (17) in Eq. (28), we obtain

$$h(\boldsymbol{\sigma}, \boldsymbol{\varepsilon}_p) = \min_{\boldsymbol{\varepsilon}} \left(\frac{1}{2} (\boldsymbol{\varepsilon} - \boldsymbol{\varepsilon}_p) : \mathbb{C} : (\boldsymbol{\varepsilon} - \boldsymbol{\varepsilon}_p) + \frac{1}{3} H_0 \, \boldsymbol{\varepsilon}_p : \boldsymbol{\varepsilon}_p - \boldsymbol{\sigma} : \boldsymbol{\varepsilon} \right). \tag{29}$$

Using the relation

$$\boldsymbol{\varepsilon} = \mathbb{S} : \boldsymbol{\sigma} + \boldsymbol{\varepsilon}_p, \tag{30}$$

the enthalpy density reads

$$h(\boldsymbol{\sigma}, \boldsymbol{\varepsilon}_p) = -\frac{1}{2}\,\boldsymbol{\sigma} : \mathbb{S} : \boldsymbol{\sigma} + \frac{1}{3}\,H_0\,\boldsymbol{\varepsilon}_p : \boldsymbol{\varepsilon}_p - \boldsymbol{\sigma} : \boldsymbol{\varepsilon}_p. \tag{31}$$

Considering a finite time interval (t_n, t), the potential Π is given by

$$\Pi = \int_\Omega h(\boldsymbol{\sigma}, \boldsymbol{\varepsilon}_p)\mathrm{d}\Omega - \int_\Omega h(\boldsymbol{\sigma}_n, \boldsymbol{\varepsilon}_{p,n})\mathrm{d}\Omega + D \tag{32}$$

where the nonnegative dissipation D for the time interval $t - t_n$ is defined as

$$D := \int_{t_n}^{t}\int_\Omega \xi\,\mathrm{d}\Omega dt \approxeq \int_\Omega \sqrt{\frac{2}{3}}\,Y\,\|\Delta\boldsymbol{\varepsilon}_p\|\,\mathrm{d}\Omega \geq 0. \tag{33}$$

with plastic strain increments

$$\Delta\boldsymbol{\varepsilon}_p = \boldsymbol{\varepsilon}_p - \boldsymbol{\varepsilon}_{p,n} \tag{34}$$

By inserting Eqs. (31) and (33) in Eq. (32), we arrive at the constrained optimization problem

$$\int_\Omega \left(-\frac{1}{2}\,\boldsymbol{\sigma} : \mathbb{S} : \boldsymbol{\sigma} - \boldsymbol{\sigma} : \boldsymbol{\varepsilon}_p + \frac{1}{3}\,H_0\,\boldsymbol{\varepsilon}_p : \boldsymbol{\varepsilon}_p + \sqrt{\frac{2}{3}}\,Y\,\|\Delta\boldsymbol{\varepsilon}_p\|\right)\mathrm{d}\Omega \longrightarrow \min_{\boldsymbol{\varepsilon}_p}\max_{\boldsymbol{\sigma},-\operatorname{div}\boldsymbol{\sigma}=\boldsymbol{f}}. \tag{35}$$

A variation of the Lagrangian functional

$$\begin{aligned}\mathcal{L}(\boldsymbol{\sigma}, \boldsymbol{\varepsilon}_p, \mathbf{u}) = &-\int_\Omega \left(\frac{1}{2}\,\boldsymbol{\sigma} : \mathbb{S} : \boldsymbol{\sigma} + \boldsymbol{\sigma} : \boldsymbol{\varepsilon}_p + \boldsymbol{f}\cdot\boldsymbol{u} - \frac{1}{3}H_0\,\boldsymbol{\varepsilon}_p : \boldsymbol{\varepsilon}_p - \sqrt{\frac{2}{3}}\,Y\,\|\Delta\boldsymbol{\varepsilon}_p\|\right)\mathrm{d}\Omega \\ &- \langle\operatorname{div}\boldsymbol{\sigma}, \mathbf{u}\rangle \longrightarrow \min_{\boldsymbol{\varepsilon}_p}\min_{\boldsymbol{u}}\max_{\boldsymbol{\sigma}}\end{aligned} \tag{36}$$

leads to a variational formulation. To solve the problem, we propose a regularization of the non-differentiable dissipation function. The used regularization technique is discussed in detail in [9, Section 12.4].

5 Numerical investigation

The following two examples, in the framework of small strain elasto-plasticity, are considered to demonstrate the performance of the TDNNS-method in combination with the notion of a dissipation function. First, we study a cantilever beam subjected to a transverse tip force. The displacement at the free edge under kinematic hardening condition is considered in a full load cycle. As a second example, we consider the well-known problem of Cook's membrane. In both examples, a convergence study for displacement quantities is conducted. For this purpose, the TDNNS-method combined with the notion of a dissipation function, as presented in the previous chapters, is implemented in the open source finite element software *Netgen/NGSolve*. The number of the elements is increased until convergence is reached. Unless stated otherwise, second order elements are used. Our

results are compared to results obtained with the commercial software tool *ABAQUS* 6.14. In *ABAQUS*, we create models with a fine discretization, which guarantees high accuracy. The TDNNS elements are also compared with standard displacement-based elements using the principle of maximum dissipation implemented in *Netgen/NGSolve*.

5.1 Cantilever beam

A thin cantilever beam, depicted in Fig. 1, clamped on the left hand side and subjected to a transverse force t_z on the right hand side, is studied. The material properties and dimensions are listed in Tab. 1. In order to examine the convergence rate of mesh refinements in $x-$direction (see Fig. 2), the deflection of the free end during a loading and unloading cycle is analyzed. The first discretization uses structured quadrilaterial meshes (Fig. 2a), the second one is a graded mesh that is refined towards the clamped end (Fig. 2b). Meshes with $2 \times 1 \times 1$, $4 \times 1 \times 2$, $8 \times 1 \times 4$ and $16 \times 1 \times 8$ grids are used for the TDNNS- and the standard-method in *Netgen/NGSolve*. The reference solution in *ABAQUS* uses quadratic elements (20 node quadratic brick), reduced integration and approximately 1.7×10^6 degrees of freedom with eight elements across the thickness. The load-deflection curve of the reference solution compared with the TDNNS-method refined towards the clamped end, illustrated in Fig. 3, show a good correlation. points A and B specify the loadsteps at which the deflection is evaluated. In both methods, about 40 loadsteps in a loading-unloading cycle are considered. The relative error of the deflection obtained with the TDNNS and the standard-method compared to the *ABAQUS* reference solution is evaluated at point A after loading and point B after unloading for different discretizations, as can be seen in Fig. 4. As expected, the relative error decreases as the spatial resolution and the number of degrees of freedom inscrease.

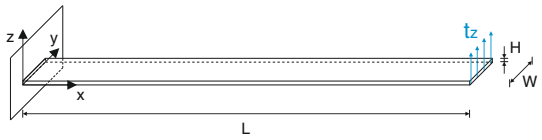

Figure 1: Geometry of the cantilever beam.

Material setup		
Dimensions	$L = 100$, $W = 10$, $H = 1$	[mm]
Young's modulus	210000	[MPa]
Poisson's ratio	$\nu = 0.3$	
Yield stress	$Y = 240$	[MPa]
Hardening modulus	$H = 7000$	[MPa]

Table 1: Cantilever beam: material parameters and dimensions.

(a) (b)

Figure 2: Cantilever beam: different meshes in x-direction, (a) structured quadrilaterial mesh and (b) refinement towards the clamped left side.

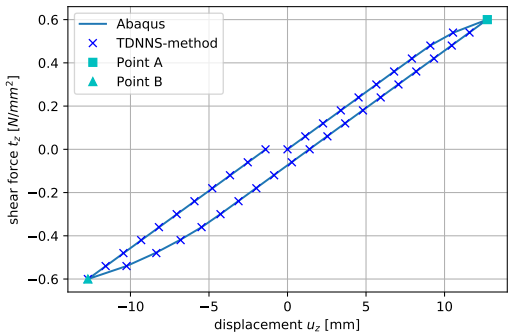

Figure 3: Cantilever beam: load-deflection curve generated with *ABAQUS* and the TDNNS method (refined towards the clamped end, second order elements).

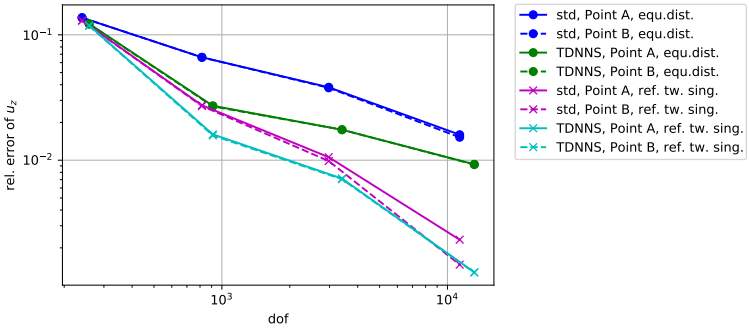

Figure 4: Cantilever beam: relative error of the deflection compared to *ABAQUS* reference solution evaluated at loadpoint A after loading and loadpoint B after unloading for different mesh refinements.

5.2 Cook's Membrane

As a second example, the well-known Cook's membrane problem is considered, see Fig. 5. The material properties and dimensions are listed in Tab. 2. Two different discretizations are considered for the analysis in *Netgen/NGSolve*. The first one uses structured quadrilaterial meshes and the second mesh is refined towards the singularity at the upper left corner. Meshes with grids $n \times n$, $n = 3, 4, \dots 20$ in x and z-directions with only one element in thickness direction are used. The convergence behavior for the displacement u_z in the upper right corner, at point A in Fig. 5, is studied. Again, a reference solution wih *ABAQUS* (20 node quadratic brick, reduced integration) with approximately 1.6×10^6 degrees of freedom and four element layers across the thickness is created. In Fig. 6, load-displacement curves of the reference solution and the TDNNS-method with various numbers of loadsteps are illustrated. The results of the vertical displacement in point A for a various number of elemens per side is depicted in Fig. 7. We observe a good agreement of the *ABAQUS* results and the TDNNS-method with 5 and 20 loadsteps. The relative errors of the displacement u_z, obtained with the TDNNS- and the standard displacement-based elements with respect to the *ABAQUS* solution for both mesh refinements and various mesh grids are depicted in Fig. 8. A significant difference is noted if the mesh is refined towards the singularity. Using a graded mash, as little as 3×3 elements are sufficient to a obtain relative error below 1% with TDNNS elements. Displacement-based elements show relative errors of more than 5% with second order ($p = 2$) elements and more than 2% with third order ($p = 3$) elements. In Fig. 9, the plastic strain componont ε_{xx} of the TDNNS-method with a mesh grading towards the singularity (3×3 grid and 8×8 grid) and of the *ABAQUS* reference solution is illustrated.

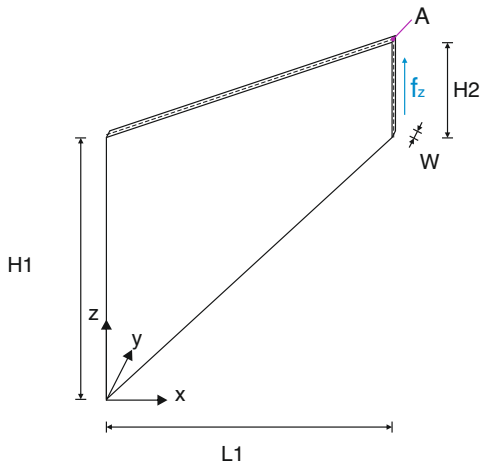

Figure 5: Geometry of Cook's membrane.

Dimensions	$L1 = 48$, $H1 = 44$	[mm]
	$H2 = 16$, $W = 1$	[mm]
Point A	$A = (48, 60, 0.5)$	[mm]
Young's modulus	206900	[MPa]
Poisson's ratio	$\nu = 0.29$	
Yield stress	$Y = 450$	[MPa]
Hardening modulus	$H = 129240$	[MPa]
Shear force f	350	[N/mm^2]

Table 2: Cook's membrane: material parameters and dimensions.

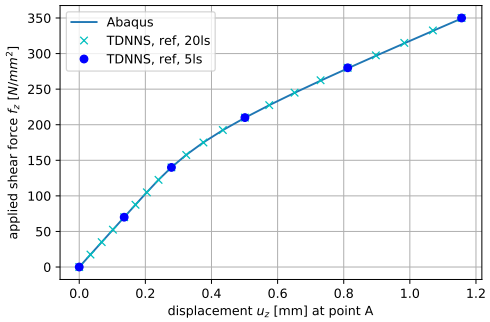

Figure 6: Cook's membrane: vertical displacement at cornerpoint A for different load steps.

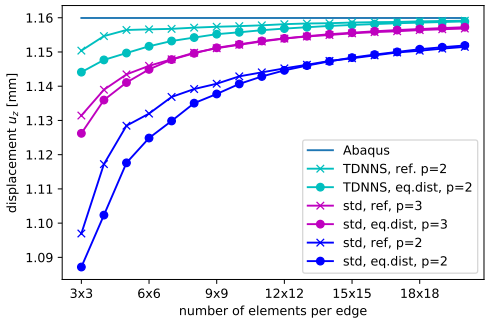

Figure 7: Cook's membrane: vertical displacement u_z at cornerpoint A for different mesh sizes.

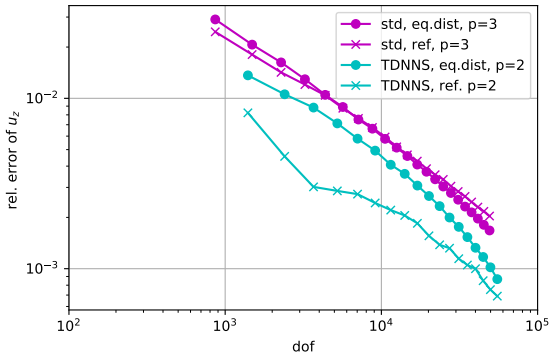

Figure 8: Cook's membrane: relative error of vertical displacement over the number of coupling degrees of freedom (dof).

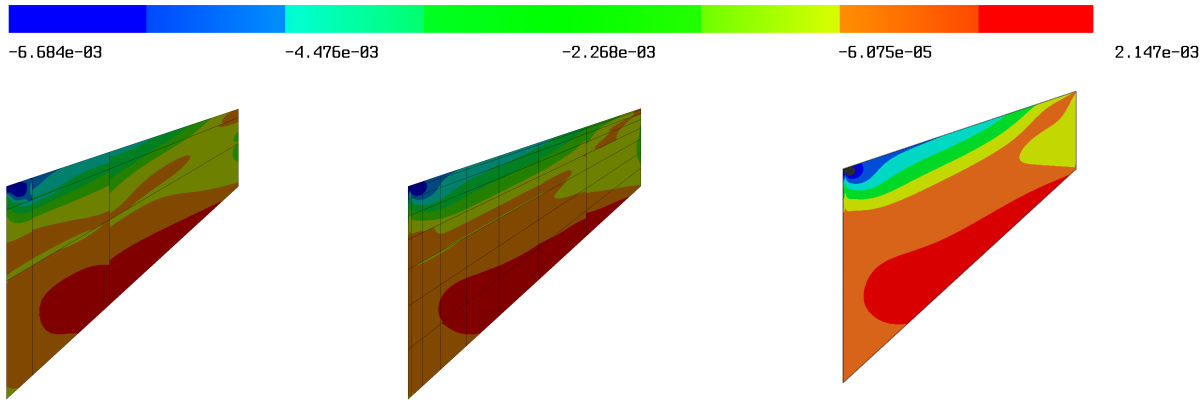

(a) (b) (c)

Figure 9: Cook's membrane: plastic strain component ε_{xx} with *Netgen/NGSolve* (a) 3×3 grid, (b) 8×8 grid and (c) *ABAQUS* reference solution.

Acknowledgement

This work has been supported by the Linz Center of Mechatronics (LCM) in the framework of the Austrian COMET-K2 program.

REFERENCES

[1] *ABAQUS/Standard User's Manual, Version 6.14*. Dassault Systèmes Simulia Corp, United States, 2014.

[2] E. Reissner. On a variational theorem in elasticity. *Journal of Mathematics and Physics*, 29(1-4):90–95, 1950.

[3] E. Hellinger. Encyklopädie der mathematischen Wissenschaften mit Einschluss ihrer Anwendungen. 4, 1913.

[4] K. Washizu. Variational methods in elasticity and plasticity. *Pergamon press Oxford*, 3, 1975.

[5] N. Viebahn, K. Steeger, and J. Schröder. A simple and efficient Hellinger Reissner type mixed finite element for nearly incompressible elasticity. *Computer Methods in Applied Mechanics and Engineering*, 340:278–295, 2018.

[6] A.S. Pechstein and J. Schöberl. Tangential-displacement and normal–normal-stress continuous mixed finite elements for elasticity. *Mathematical Models and Methods in Applied Sciences*, 21(08):1761–1782, 2011.

[7] A.S. Pechstein and J. Schöberl. Anisotropic mixed finite elements for elasticity. *International journal for numerical methods in engineering*, 90(2):196–217, 2012.

[8] J. Lubliner. *Plasticity theory*. Courier Corporation, 2008.

[9] W. Han and B.D. Reddy. *Plasticity: Mathematical theory and numerical analysis*, volume 9. Springer Science & Business Media, 2012.

[10] G.A. Maugin. *The thermomechanics of plasticity and fracture*, volume 7. Cambridge University Press, 1992.

[11] R. Hill. *The mathematical theory of plasticity*, volume 11. Oxford university press, 1998.

[12] J.C. Simo and T.J.R Hughes. *Computational inelasticity*, volume 7. Springer Science & Business Media, 2006.

[13] M.L. Wilkins. Calculation of elastic-plastic flow. Technical report, California Univ Livermore Radiation Lab, 1963.

[14] J.C. Simo. Numerical analysis and simulation of plasticity. *Handbook of numerical analysis*, 6:183–499, 1998.

[15] A.R. Srinivasa. Application of the maximum rate of dissipation criterion to dilatant, pressure dependent plasticity models. *International journal of engineering science*, 48(11):1590–1603, 2010.

[16] J. Schröder, M. Igelbüscher, A. Schwarz, and G. Starke. A Prange–Hellinger–Reissner type finite element formulation for small strain elasto-plasticity. *Computer Methods in Applied Mechanics and Engineering*, 317:400–418, 2017.

[17] J.C. Simo, J.G Kennedy, and R.L. Taylor. Complementary mixed finite element formulations for elastoplasticity. *Computer Methods in Applied Mechanics and Engineering*, 74(2):177–206, 1989.

[18] J.C. Nédélec. Mixed finite elements in R^3. *Numerische Mathematik*, 35(3):315–341, 1980.